Mixed-mode cohesive-zone models for fracture of an adhesively-bonded polymer-matrix composite

S. Li[1], M. D. Thouless[1,2], A. M. Waas[3], J. A. Schroeder[4], and P. D. Zavattieri[4]

[1]*Department of Mechanical Engineering*
[2]*Department of Materials Science & Engineering*
[3]*Department of Aerospace Engineering*
University of Michigan, Ann Arbor, MI 48109

[4]*General Motors Research and Development*
Warren, MI 48090

Abstract

As a direct extension of previous mode-I work on the adhesion of composite joints, this paper uses a cohesive-zone approach to model the mixed-mode fracture of adhesive joints made from a polymer-matrix composite. Mode-II cohesive-zone parameters were obtained using sandwich end-notch flexure specimens. These parameters were used directly with the previously-determined mode-I parameters to predict the fracture and deformation of mixed-mode geometries. It was shown that numerical simulations provided quantitative predictions for these geometries, including predictions for both the strengths of the joints and for the failure mechanisms. In conjunction with the earlier work, these results demonstrate the use of cohesive-zone approaches for the design of adhesively-bonded composite joints, and indicate approaches for determining the relevant material properties to describe mixed-mode fracture.

(June 2005)

Keywords: cohesive zone, mixed-mode fracture, composite, adhesive, failure mechanism

1. Introduction

Adhesive bonding technology is used in a variety of industries including the automotive, aerospace and semiconductor industries. However, design approaches for predicting the fracture of adhesively-bonded materials are still somewhat empirical, and improving these approaches is a critical issue for furthering the engineering applications of this technology. The most common approach for analyzing the fracture of adhesive joints is the use of interfacial fracture mechanics, which uses an energy parameter (toughness) as the failure criterion. In principle, it is possible to characterize the toughness of an interface as a function of the relative amounts of normal and shear deformation acting at the crack tip. Provided the interface in an adhesive joint contains a well-defined crack, and the deformation of the system is dominated by linear elastic deformation of the adherends, it is possible to use mixed-mode fracture mechanics to calculate the strength of the joint under different loading conditions [Hutchinson and Suo, 1992]. However, this energy-based approach relies on the existence of a crack in the interface, and on assumptions of small-scale bridging and linear-elasticity. If any of these conditions are violated, an alternative approach such as cohesive-zone modeling is required [Needleman, 1987; Ungsuwarungsri and Knauss, 1987; Tvergaard and Hutchinson, 1992].

Previous papers [Sørensen, 2002; Sørensen and Jacobsen, 2003; Li *et al.*, 2005b] have shown that cohesive-zone models can provide quantitatively predictive analyses for the mode-I fracture of adhesively-bonded composite joints. An important concept of the cohesive-zone approach is that both strength and energy parameters are used to characterize the debonding process along the fracture plane, allowing the approach to be of much more general utility than conventional interfacial fracture mechanics. The present paper extends the earlier work of Li *et al.* [2005b] on mode-I fracture by focusing on determining the mode-II cohesive parameters for an adhesively-bonded composite system. These parameters are then used in conjunction with the mode-I parameters to verify the predictive capabilities of the cohesive-zone approach for mixed-mode geometries.

2. Specimen preparation and characterization of the materials

The composite used for the adherends in this study was the polypropylene matrix with randomly-oriented glass fibers that has been described in an earlier paper [Li *et al.*, 2005a].[1] The volume fraction of the fibers was about 19%. The as-received material was remolded using a hydraulic press at 70 °C and 13 MPa for about 1.5 minutes. Details of the constitutive properties of the composite, and how they were obtained, have been described elsewhere [Li *et al.*, 2005a]. While there was considerable variability in the mechanical properties, the composite could be approximated as being transversely isotropic and elastic / perfectly-plastic in plane, with an in-plane tensile modulus of $E = 6.0 \pm 1.5$ GPa, an in-plane Poisson's ratio of 0.30 ± 0.03, and an in-plane shear yield strength of 65 ± 15 MPa. Additionally, the out-of-plane tensile modulus was 4 ± 1GPa, while the out-of-plane shear modulus was 0.5 ± 0.1 GPa [Sun, 2004].

[1] Azdel R401 provided by Azdel, Inc.

The adhesive used to bond the coupons was the same experimental, two-part material used in the prior mode-I studies [Li *et al.*, 2005b].[2] This adhesive cured at room temperature, and was specially formulated to bond low-surface-energy materials such as polypropylene. Before bonding, the composite surfaces were wiped clean to remove any dirt or debris (no mold-release agent had been used when forming the composite coupons). During bonding, the adhesive layer was kept at a uniform thickness of 0.6 ~ 0.8 mm by using glass beads as spacers. Where required, a strip of Teflon tape was inserted into one of the adhesive/composite interfaces before applying the adhesive, so as to define the limits of the adhesive.

Preliminary mode-II fracture tests with the bonded composites showed that it was extremely difficult to obtain stable interfacial crack propagation, as the composite arms tended to fail after only limited amounts of crack growth (Fig. 1). Therefore, metal arms were bonded to the composite forming sandwich specimens which were used to determine the mode-II cohesive parameters. This had two beneficial effects arising from the relatively high stiffness and strength of the metal compared to the composite. First, extensive interfacial crack propagation could be obtained before the composite failed. Second, the effects of the variability in the modulus of the composite were suppressed because the stiffness of the bonded structures was dominated by the metal. The particular metals chosen in this study were a cold-rolled steel and an aluminum 5754 alloy. Since it was crucial to know the constitutive properties of the metal arms accurately when analyzing the sandwich specimen, stress-strain curves for the

[2] Provided by Dow Chemical Company.

steel and aluminum were obtained from standard uniaxial tensile tests. These curves are shown in Fig 2a and Fig. 2b, respectively, and the constitutive properties of both the steel and the aluminum were incorporated into the subsequent numerical calculations directly as point-to-point representations of these data. Both metals were modeled as being isotropic, with a von Mises yield criterion for the onset of yield.

3. Mixed-mode cohesive-zone models

To characterize the fracture behavior of the mixed-mode geometries, a mode-dependent cohesive-zone model was developed. The cohesive-zone model was implemented in ABAQUS through user-defined elements and associated sub-routines. Following the mixed-mode model of Yang and Thouless (2001), the entire adhesive layer was replaced by user-defined, cohesive-zone elements, and it was assumed that opening and shear traction-separation laws were totally unrelated, except being coupled through a simple failure criterion of the form

$$\mathcal{G}_1 / \Gamma_I + \mathcal{G}_{II} / \Gamma_{II} = 1. \qquad (1)$$

Here Γ_I and Γ_{II} (the mode-I and mode-II toughness) represent the total areas under the traction-separation curve for each mode, and the mode-I and mode-II energy-release rates are given by

$$\mathcal{G}_I = \int_0^{\delta_{nc}} \sigma(\delta_n) d\delta_n ; \qquad \mathcal{G}_{II} = \int_0^{\delta_{tc}} \tau(\delta_t) d\delta_t \qquad (2)$$

where δ_n and δ_t are the normal and shear displacements, σ and τ are the normal and shear tractions, and δ_{nc} and δ_{tc} are the critical normal and shear displacements. The numerical calculations proceeded by computing Eqns. (2) for both modes until the failure condition of Eqn. (1) was met and the crack advanced; at this point the element was considered to be no longer capable of bearing a load, and the tractions acting on the element were set to zero. Mesh sensitivity analyses were conducted to ensure that any numerical effects on the results were less significant than effects from other sources of uncertainty, such as the variability of experimental results. The lengths of the cohesive-elements were at least 25 times smaller than the adherend thickness, *h*, and at least five times smaller than δ_{nc} and δ_{tc}. Additional details of the numerical techniques are provided in the accompanying Ph.D. thesis [Li, 2004].

Descriptions of the mode-I fracture properties of the adhesive interface, and how they were obtained, have been previously described in Li *et al.* [2005b]. In that reference it was shown that the phenomenon of fiber pull-out during mode-I fracture resulted in a clear distinction between what was termed the characteristic strength and the cohesive strength of the interface. The cohesive strength of the interface was identified as the maximum stress that the interface could support, while the characteristic strength was identified as the value of the strength that, in conjunction with the toughness, controlled crack propagation. (Alternatively, the characteristic strength can be thought of as the parameter that in conjunction with the value of the critical opening displacement of the cohesive zone establishes the toughness, or an average strength.) The need to distinguish between the two strength values was equivalent to a recognition that there are some circumstances under which the shape of the cohesive law has an influence on the fracture of an interface. The three-parameter mode-I traction-separation law that was obtained in Li *et al.* [2005b] to describe the fracture of the adhesive interface used in the present study is shown in Fig. 3a. This traction-separation law represents interfacial cracking followed by fiber pull-out, and the three important parameters that describe the law are the cohesive strength of the interface, $\hat{\sigma}_{io}$ =24 ± 3 MPa, the characteristic strength of the interface, $\hat{\sigma}_i$ = 5.0 ± 1.5 MPa, and the toughness, Γ_{Ii} = 7.3 ± 1.8 kJm^{-2}. This mode-I law was used without any further modification in the present work.

In contrast to the mode-I behavior, preliminary mode-II tests indicated that few fibers were pulled out during mode-II fracture. Therefore, a simple trapezoidal traction-separation law of the form shown in Fig. 3b, in which the characteristic strength and cohesive strength are essentially identical, was chosen to simulate elastic/plastic behavior of the adhesive for the mode-II debonding process (Kafkalidis *et al*., 2000). The initial slope of the traction-separation law was chosen to mimic the shear stiffness of the adhesive layer, and the unloading slope was selected for computational ease, since experience has shown that the precise details of this slope are generally not very significant. Since, under some loading configurations, the cohesive elements can experience negative displacements, linear-elastic behavior was assumed in the compressive regime for the normal loading mode, and a trapezoidal law mirroring the response for positive displacements was assumed for negative displacements in the shear loading mode (Fig. 3).

4. Determination of the mode-II interfacial cohesive parameters

4.1 Interfacial shear tests

To investigate the shear strength of the interface, specimens of the form shown in Fig. 4 were fabricated. Two coupons of the composite were bonded together using the experimental adhesive. Since the shear properties of the adhesive layer were expected to be sensitive to the bond-line thickness [Chai, 1993], glass spheres were used as spacers to ensure that the bond-line thickness was always maintained at a constant value of 0.7 ± 0.1 mm in all specimens. The interface between the adherends was then machined to leave a short ligament of about 5.5 mm between the two coupons. A shear load was applied, as shown in Fig. 4, by means of a screw-driven testing machine at a displacement rate of 0.4 mm/minute. The average strength, defined as the maximum applied load divided by the bonded area, was determined to be 13 ± 3 MPa. A numerical stress analysis using ABAQUS 6.3 with continuum elements representing the constitutive properties of the adhesive [Li *et al.*, 2005b] confirmed that the distribution of the shear stress across the adhesive layer was approximately uniform, so that the average shear strength measured in this fashion is expected to be reasonably representative of the cohesive shear strength.

4.2 Sandwich end-notched flexure tests

An example of a mode-II geometry is the three-point-bending end-notched-flexure (ENF) specimen. In this geometry, the deformation at the crack-tip is dominated by shear, with a limited amount of compressive normal stresses. Thus, the geometry provides an excellent configuration to study pure mode-II fracture behavior [Barret and Foschi, 1977; Chiang and Chai, 1994, Yang *et al.*, 2001). Sandwich end-notched flexure (SENF) specimens with the geometry shown in Fig. 5 were fabricated by cutting coupons of the composite and steel, and then bonding them with the adhesive, maintaining the bond-line thickness at 0.7 ± 0.1 mm. To facilitate experimental observations, straight lines were cut vertically across the bond-lines using a sharp razor. During the test, the specimen rested on two steel cylinders. A similar cylinder was used to load the specimen at its mid-point. To reduce possible frictional effects along the cracked surfaces, a steel wire with a diameter of about 0.8 mm was inserted as a spacer between the arms of the adherends at the crack mouth. The specimens were tested under displacement control with a cross-head velocity of 0.6 mm/minute under ambient conditions. A high-resolution CCD camera was used to correlate the mid-point displacement to the cross-head displacement, as well as to monitor crack propagation.

Figure 6 shows examples of the relationship between the applied load and the deflection of the mid-point of the beam. Although there appears to be two different types of behaviors (monotonically increasing curves and curves with a primary maximum), no correlation with details of the geometry of the specimens was noted. Optical micrographs of the side of the specimens are shown in Fig. 7. Although the precise location of crack tip is difficult to identify from these views, the extent of shear along the interface can be seen. Examination of the crack surfaces after fracture indicated that crack growth was purely interfacial, and that relatively few fibers were pulled out during fracture; this was consistent with the preliminary tests mentioned earlier.

4.4 Numerical simulations

To extract the mode-II cohesive properties of the interface, the finite-element code ABAQUS (version 6.3) was used to perform a cohesive-zone analyses of the sandwich geometry. The calculations were conducted allowing non-linear displacements of the adherends. The adherends were modeled by a continuum finite-element model of the SENF geometry, using the appropriate constitutive properties for the steel and the composite, as described earlier. To prevent interpenetration at the crack mouth, surfaced-based contact elements were used to simulate the interaction between the steel spacer and the two arms. The adhesive layer between the metal arms and the composite was modeled using continuum elements with the adhesive constitutive properties [Li *et al.*, 2005b]. The adhesive layer bonding the composite layers together was replaced by four-noded mixed-mode cohesive-zone elements [Li, 2004] with an initial thickness of 0.7 mm. As discussed earlier, the mode-II interfacial fracture was characterized by a simple trapezoidal traction-separation law of the form shown in Fig. 3b, with an initially unknown shear strength and mode-II toughness. The mode-I parameters previously obtained for the adhesive (Fig. 3a) were used without any further modification. [3] The mode-I and mode-II traction-separation laws were coupled through the failure condition of Eqn. 1.

The two unknown mode-II parameters were obtained by a parametric study that compared the results from numerical calculations for the load-displacement curves with the experimental results of Fig. 6. It was observed from the numerical calculations that the final rising part of the curves is dominated by the mode-II toughness. Therefore, the mode-II toughness could be obtained by matching the numerical predictions and the experimental results in this region. This comparison indicated that $\Gamma_{IIi} = 11.5 \pm 1.5$ kJm^{-2}. Once the toughness had been determined, the corresponding shear strength was found by adjusting the maximum stress in the traction-separation law, while keeping the toughness fixed, until the full load-displacement curve could be fitted to the experimental data. This analysis resulted in a value of $\hat{\tau}_i = 12 \pm 1.5$ MPa, which is in excellent agreement with the average shear strength obtained from the interfacial shear tests discussed earlier, and supports the notion that, unlike the mode-I law, no distinction needs to be drawn between the cohesive strength and the characteristic strength. The numerical fit for how the applied load varies with the mid-point deflection using the mode-II cohesive parameters is compared with the experimental results in Fig. 8. As can be seen from the plot, the numerical results provide excellent quantitative reproduction of the experimental results, in the sense that they closely bracket them. The fits provide a reasonable uncertainty of less than about 15% in the values of the cohesive parameters, which mirrors the experimental uncertainty.

The cohesive law used for in these studies resulted in load-displacement curves with a primary maximum. While this shape was obtained for some of the experimental results, monotonic load-displacement curves were also obtained experimentally. The fact that the numerical curves fitted the general form and scale of the load-displacement curves, without completely capturing the details,

---

[3] The numerical calculations confirmed that the SENF geometry did deform under pure mode-II conditions, with the normal stresses at the crack tip being slightly compressive.

probably illustrates that, while a characteristic strength and toughness are generally sufficient to model the behavior at a level suitable for design purposes, capturing nuances of the load-deflection curves may require knowledge of the precise shape of the traction-separation law. However, such additional sophistication will come at the expense of additional parameters that need to be determined with additional experiments. Exploring this concept in detail was beyond the scope of what was being attempted in the present paper, which had the goal of establishing a methodology to determine cohesive parameters at a level suitable for design purposes, rather than capturing nuances in load-displacement curves. However, an additional series of numerical calculations indicated that it was indeed possible to reproduce both types of curve by changing the shape of the traction-separation law. Decreasing the cohesive strength or reducing the relative displacement at which unloading of the traction-separation law begins seemed to favor a more monotonic form of curve over the curves with a primary maximum. For example, a traction-separation law where unloading began at $0.1\delta_{tc}$, rather than $0.6\delta_{tc}$, with $\Gamma_{II} = 10$ kJm^{-2} and $\hat{\tau}_i = 13$ MPa, allowed an almost perfect fit to the experimental monotonic load-displacement curves.

5. Verification of mixed-mode fracture

5.1 Numerical predictions of sandwich single-lap-shear tests

Earlier work showed that pure mode-I behavior could be modeled by a cohesive-zone model [Li *et al.*, 2005b]; the previous section has presented results for what was essentially pure mode-II fracture (even though a full mixed-mode analysis was used). In this section, the use of the mode-I and mode-II interface parameters to investigate a mixed-mode configuration is demonstrated. The configuration investigated was a lap-shear geometry consisting of the composite bonded to an aluminum alloy (Fig. 9). The aluminum arms were 2.0 mm thick, and the composite coupons in these specimens were 2.8 mm thick. Two different bonded over-lap lengths, 40 mm and 50 mm, were used; the width of the specimens was 20mm and the free portion of the arms was 30 mm.

The numerical simulations were done using the constitutive properties of the composite and aluminum described earlier. The adhesive layer was modeled using cohesive elements with the appropriate mode-I and mode-II parameters (Table 1), along with the failure criterion of Eqn. (1). This combination of geometry and cohesive parameters was shown to be mixed-mode with a ratio of $\mathcal{G}_{II}/\mathcal{G}_{I}$ at fracture of about 2. The numerical simulations showed stable crack propagation for about 8 mm before unstable failure occurred, with crack propagation being accompanied by macroscopic plastic deformation of the aluminum. The predicted peak load (per unit width) was in the range of 400 Nmm^{-1} to 570 Nmm^{-1} for the 40 mm overlap length, and between 510 Nmm^{-1} and 710 Nmm^{-1} for the 50 mm overlap length. The upper and lower bounds for the predicted loads corresponded to the upper and lower bounds of the cohesive parameters (Table 1).

5.2 Experimental verification

Sandwich single-lap shear specimens with dimensions identical to the geometries analyzed numerically were tested to verify these numerical predictions. The lap-shear specimens were tested in a screw-driven machine at a displacement rate of 1.0 mm/minute, with displacements being measured optically between two points separated by a gauge length of 80 mm using a C.C.D camera. It was observed that, in all cases, the fracture of the sandwich specimens was purely interfacial, as assumed for the numerical simulations. The specimens showed stable crack growth for about 13 mm before catastrophic failure occurred. Figures 10(a) and 10(b) compare the numerical predictions with the experimental load-displacement curves for the two different geometries. The experimental data are shown as points corresponding to optical measurements of the displacement; the solid lines are the numerical predictions. The deformation of the aluminum sandwich specimen (with an overlap length of 40 mm) immediately before catastrophic failure is compared to the deformation predicted by the numerical calculations in Fig. 11. It should be emphasized at this point that the numerical results in Fig. 10 are *predictions* done in isolation from the experiments. They were *not* attempts to *reproduce* the experimental results, and should be contrasted with the calculations of Fig. 8 which were performed to obtain material parameters by fitting experimental results. The range of the numerical predictions in Fig. 10 represents what is expected to be the full range of the effects of uncertainties in both the mode-I and mode-II cohesive parameters. The results of individual experiments are expected to fall within the predicted range. In particular, statistical effects are probably responsible for the reason why the few experimental results do not show the full range of predicted variability.

6. Fracture of composite joints

As described at the beginning of the paper, the preliminary tests showed that end-notched flexure specimens which were not bonded to a metal failed by fracture of the composite arms (see Fig. 1). Now, it is of interest to see whether this behavior can be reproduced numerically using the cohesive properties of the interface and the mode-I cohesive properties of the composite (Fig. 12 and Table 1) obtained in an earlier work [Li *et al.*, 2005a]. Although, it is clear from Fig. 1 that an accurate prediction of the complete crack path in the composite would require the mode-II properties of the composite to be included in any model, the experimental observations indicate that failure in the composite starts off along a mode-I trajectory. Therefore, it can be assumed that only the mode-I properties of the composite are needed to investigate when cracking begins in the composite.

The dimensions for the ENF geometry are shown in Fig. 13: the span, $2L$, was 140 mm, and the initial crack length, a, was 30 mm, the composite thickness, h, was 7.6 mm, and the adhesive layer thickness was 0.7 mm. A calculation in which both the composite and interface are fully modeled by cohesive elements would be computationally intensive. Following a similar approach used for investigating the mode-I fracture of this same adhesively-bonded system, the numerical calculations were performed in two stages [Li *et al.*, 2005b]. In the first stage, the composite was modeled by its continuum properties, and the adhesive layer was replaced by the appropriate mixed-mode cohesive-zone model of the interface. These initial calculations were used to identify the direction and location of the maximum normal stresses in the arms at the conditions under which the interface crack grows. In the present case, the maximum normal stresses were approximately perpendicular to the interface. In the second stage of the calculations, cohesive-zone elements with the mode-I fracture properties of the composite (Fig. 12) were embedded in the composite near the crack tip (where the normal stresses were largest) perpendicular to the interface. The calculations were then allowed to proceed with competition between crack growth in the interface and in the composite. To keep the numerical model to a reasonable size, the region in which cohesive-zone elements were embedded was limited to 10 mm in length. If the calculation indicated that the interface crack grew out of this region without failure of the composite, the geometry was re-meshed and a new calculation was started.

The results of the numerical simulations depended on the relative magnitudes of the cohesive parameters for the strengths of the composite and interface. For a relatively weak interface and strong composite the crack could grow along the interface for about 20 mm before being arrested. A further increase in applied displacement then caused failure of the composite, without further interfacial crack growth. Conversely, composite failure before any interfacial crack growth occurred if the composite was relatively weak, or if the interface was relatively strong. A comparison of the predicted load-displacement curves with the experimental curves is given in Fig. 14. It should be noted that the numerical curves terminate at the onset of unstable crack growth in the composite. Owing to the assumptions made of pure mode-I growth in the composite, these points should more properly be considered to represent the initiation of fracture within the composite. The numerical predictions of composite failure after limited interfacial crack growth were consistent with what was observed experimentally, as are the magnitudes of the predicted strengths (which bracket the observed strengths).

7. Conclusions

The mode-II cohesive parameters for a composite / adhesive joint were determined using sandwich end-notched flexure specimens in which the composite was bonded to a metal. Such a geometry was found to be useful because the stiffness of the metal compared to the composite ensured that most of the load was born by the metal. This eliminated the tendency for the composite to fail, and also suppressed the effects of the variability of the modulus of the composite. It was observed that, for the particular system studied in this paper, the characteristic strength for the mode-II traction-separation law was essentially identical to the cohesive-strength of the interface. The average shear strength of the interface measured by direct shear was identical to the characteristic shear strength measured from fracture tests. This was in distinct contrast to the mode-I behavior of the same interface for which it was observed that the characteristic strength for crack growth was considerably lower than the cohesive strength of the interface measured by direct tensile tests. These results were consistent with observations that mode-I fracture was accompanied by extensive fiber pull-out, but that mode-II fracture was not. With both the mode-I and mode-II cohesive parameters determined for the adhesive interface, the behavior of other geometries were modeled and compared to experimental results. It was shown that the numerical results did a reasonably good job of predicting both the strengths of the joints and the failure mechanism.

Acknowledgements

S. L., M. D. T. and A. M. W. gratefully acknowledge the financial support of General Motors, the supply of the composite from Azdel, Inc., and the supply of the adhesive from Dow Chemical. The use of unpublished data by C. Sun and Z. Wu is also gratefully acknowledged.

References

Barret, J.D. and Foschi, R.O., “Mode II stress-intensity factors for cracked wood beams,” *Engineering Fracture Mechanics*, **9**, 371–378 (1977).

Chai, H., “Deformation and failure of adhesive bonds under shear loading,” *Journal of Materials Science*, **28**, 494–506 (1993).

Chiang, M.Y.M. and Chai, H., “Plastic deformation analysis of cracked adhesive bonds loaded in shear,” *International Journal of Solids and Structures*, **31**, 2477–2490 (1994).

Hutchinson, J. W. and Z. Suo, “Mixed-mode cracking in layered materials,” *Advances in Applied Mechanics*, **29**, 64-187 (1992).

Kafkalidis, M. S., M. D. Thouless, Q. D. Yang and S. M. Ward, “Deformation and fracture of an adhesive layer constrained by plastically-deforming adherends,” *J. Adhes. Sci. Technol.*, **14**, 1593-1607 (2000).

Li, S., "Fracture analysis of an adhesively-bonded polymer-matrix composite," Ph.D. dissertation, University of Michigan, Ann Arbor, MI (2004).

Li, S., M. D. Thouless, A. M. Waas, J. A. Schroeder, and P. D. Zavattieri, “Use of a cohesive-zone model to analyze the fracture of a fiber-reinforced polymer-matrix composite," *Journal of Composites Science & Technology*, **65**, 537-549 (2005).

Li, S., M. D. Thouless, A. M. Waas, J. A. Schroeder, and P. D. Zavattieri, “Use of mode-I cohesive-zone models to describe the fracture of an adhesively-bonded polymer-matrix composite,” *Journal of Composites Science & Technology*, **65**, 537-549 (2005).

Needleman, A. “A continuum model for void nucleation by inclusion debonding,” *Journal of Applied Mechanics*, **54**, 525-531 (1987).

Sørensen, B. F., “Cohesive law and notch sensitivity of adhesive joints,” *Acta Materialia,* **50**, 1053-1061 (2002).

Sørensen, B. F and T. K. Jacobsen, "Determination of cohesive laws by the J-integral approach," *Engineering Fracture Mechanics*, **70**, 1841-1858 (2003).

Sun, C., unpublished work (2004).

Tvergaard, V. and J. W. Hutchinson, "The relation between crack growth resistance and fracture parameters in elastic-plastic solids," *Journal of the Mechanics and Physics of Solids*, **40**, 1377-1397 (1992).

Ungsuwarungsri, T. and W. G. Knauss, "Role of damage-softened material behavior in the fracture of composites and adhesives," *International Journal of Fracture*, **35**, 221-241 (1987).

Wu, Z., unpublished work (2004).

Yang, Q. D., M. D. Thouless and S. M. Ward, "Elastic-Plastic Mode-II Fracture of Adhesive Joints," *International Journal of Solids and Structures*, **38**, 3251-3262 (2001).

Yang, Q. D. and M. D. Thouless, "Mixed-mode fracture analyses of plastically-deforming adhesive joints," *International Journal of Fracture*, **110**, 175-187 (2001).

Figure captions

Figure 1 Micrograph of an end-notched flexure specimen, showing composite failure **(a)** before crack propagation **(b)** after about 20 mm crack propagation.

Figure 2 The relationship between true stress and true strain for **(a)** the cold-rolled steel and **(b)** the aluminum 5754 alloy used in this study (from Wu, [2004]).

Figure 3 **(a)** Traction-separation law used to describe the mode-I fracture of the particular adhesive interface studied in this paper (from [Li *et al.*, 2005b]). **(b)** Schematic traction-separation law used to describe the mode-II fracture of this adhesive interface.

Figure 4 Configuration of the specimens used to measure the average interfacial shear strength.

Figure 5 Geometry and dimensions for the sandwich end-notched flexure specimens used to investigate the mode-II fracture properties of the adhesive-composite interface.

Figure 6 Plots of applied load *versus* center deflection for the sandwich end-notched flexure specimens with the geometry given in Fig. 5.

Figure 7 Micrographs of the side of the sandwich end-notched flexure specimens, during the course of the experiment.

Figure 8 Comparison between the numerical fits for the load-displacement curves and the experimentally observed curves of Fig. 6. The dotted lines show the experimental results, while the solid lines are the numerical fits. Numerical solutions have been shown for the average values of the mode-II cohesive properties, and for the upper and lower limits of both the toughness and shear strength.

Figure 9 Geometry and dimensions for the sandwich single-lap-shear specimens used to investigate mixed-mode fracture of the adhesive-composite interface with aluminum arms.

Figure 10 Comparison between the numerical predictions for the load-displacement curves and the experimentally observed curves for aluminum sandwich single lap shear specimens with an overlap length of **(a)** 40 ± 2 mm, and **(b)** 50 ± 2 mm. The dotted points indicate experimental data. The solid lines are numerical predictions showing upper and lower bounds based on the range of cohesive parameters.

Figure 11 Comparison between the experimentally-observed deformation and the numerically-predicted deformation of an aluminum sandwich single-lap-shear specimen with 40 mm overlap length, at the onset of catastrophic failure.

Figure 12 Traction-separation law used to describe the mode-I fracture of the composite (from [Li *et al.*, 2005a]).

Figure 13 Geometry of the end-notched flexure specimens for the adhesively bonded composite.

Figure 14 Load (per unit width) *vs.* mid-point deflection for the end-notched flexure specimens with the geometry shown in Fig. 13. The dotted lines show the experimental results, with the point of crack initiation within the composites indicated. The solid lines indicate the numerical predictions with four limits shown for (i) the strongest composite and strongest interface, (ii) the strongest composite and weakest interface, (iii) the weakest composite and the strongest interface, and (iv) the weakest composite and weakest interface.

Table 1 Summary of the interfacial and composite cohesive parameters used in this study.

Mode-I			Mode-II	
Interface			Interface	
$\hat{\sigma}_{io}$ (MPa)	$\hat{\sigma}_{i}$ (MPa)	Γ_{Ii} (kJm^{-2})	$\hat{\tau}_{i}$ (MPa)	Γ_{IIi} (kJm^{-2})
24 ± 3	5.0 ± 1.5	7.3 ± 1.8	12 ± 1.5	11.5 ± 1.5
Composite				
$\hat{\sigma}_{m}$ (MPa)	$\hat{\sigma}_{b}$ (MPa)	Γ_{Ic} (kJm^{-2})		
100 ± 20	79 ± 8	40 ± 4		

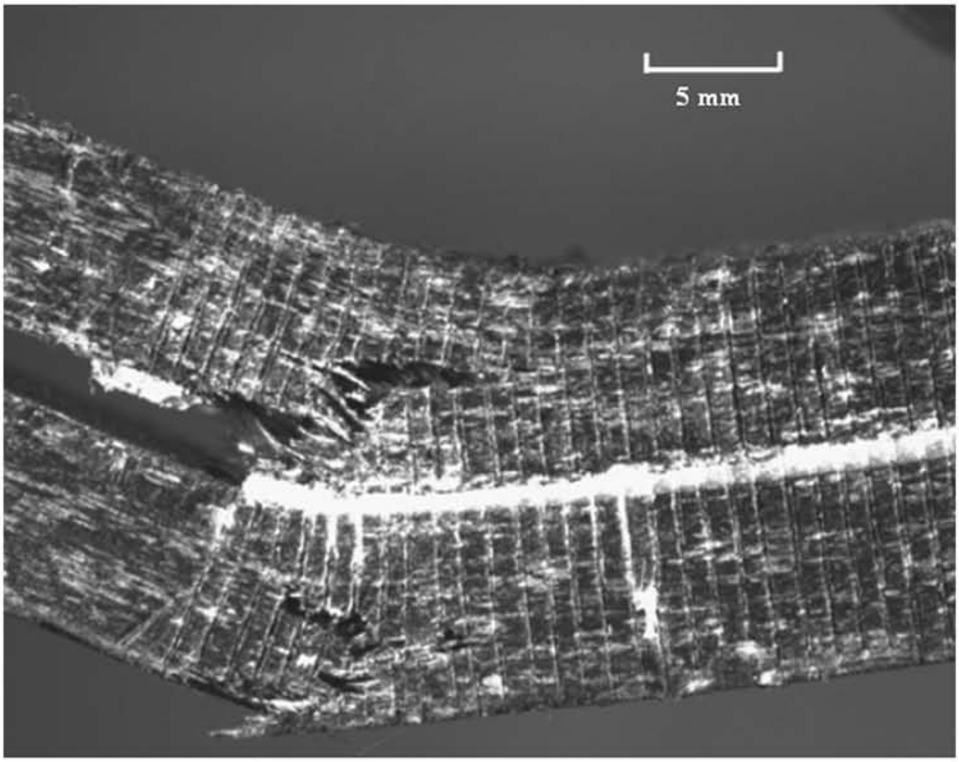

Figure 1a

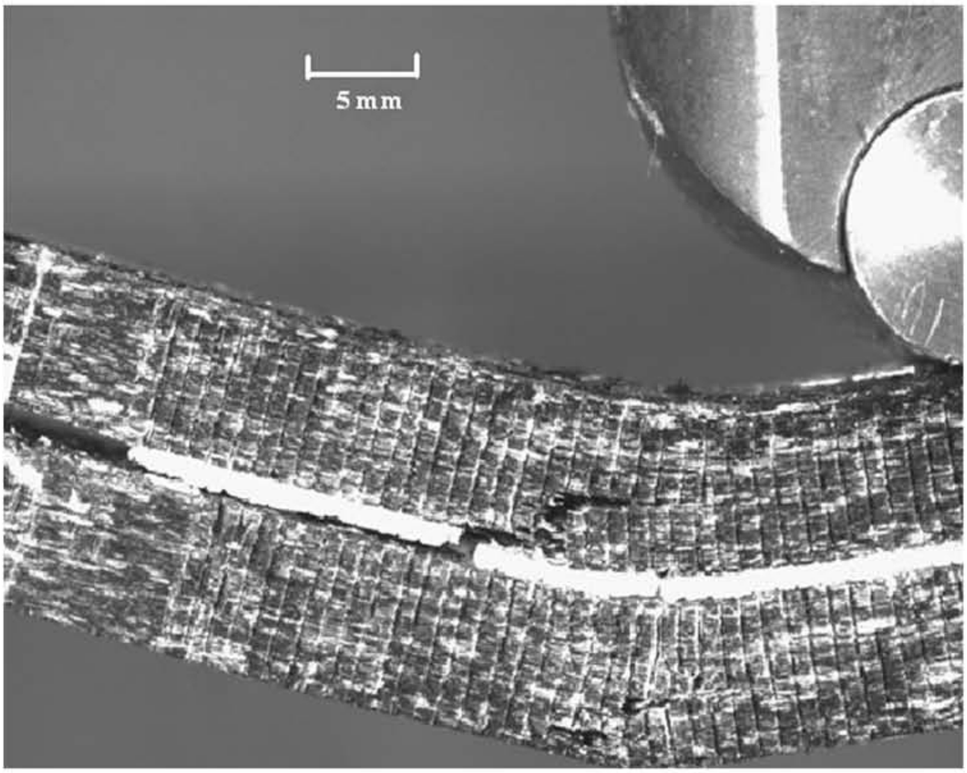

Figure 1b

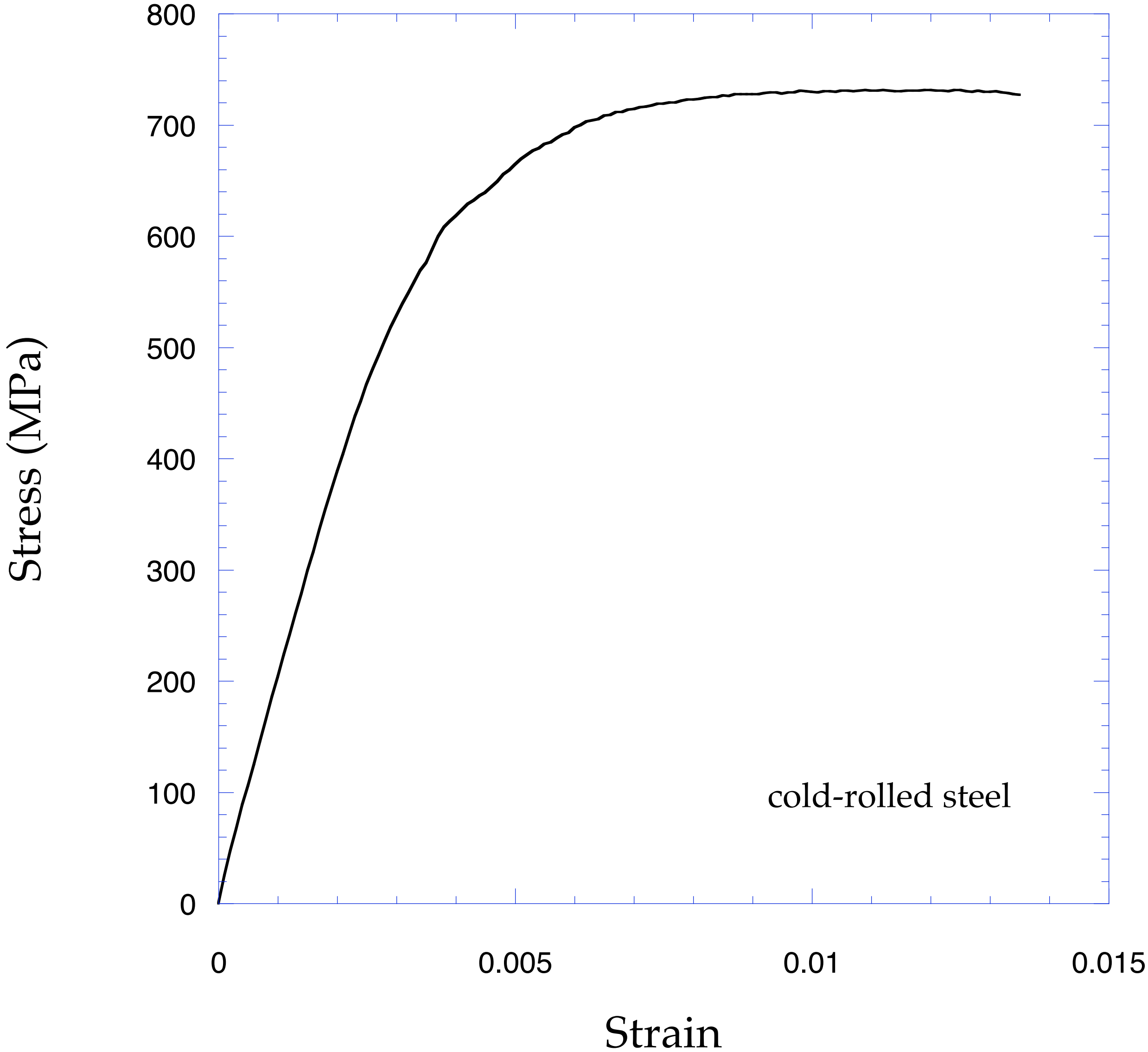

Stress (MPa)
800
700
600
500
400
300
200
100
0
0
0.005
0.01
0.015
Strain
cold-rolled steel

Figure 2a

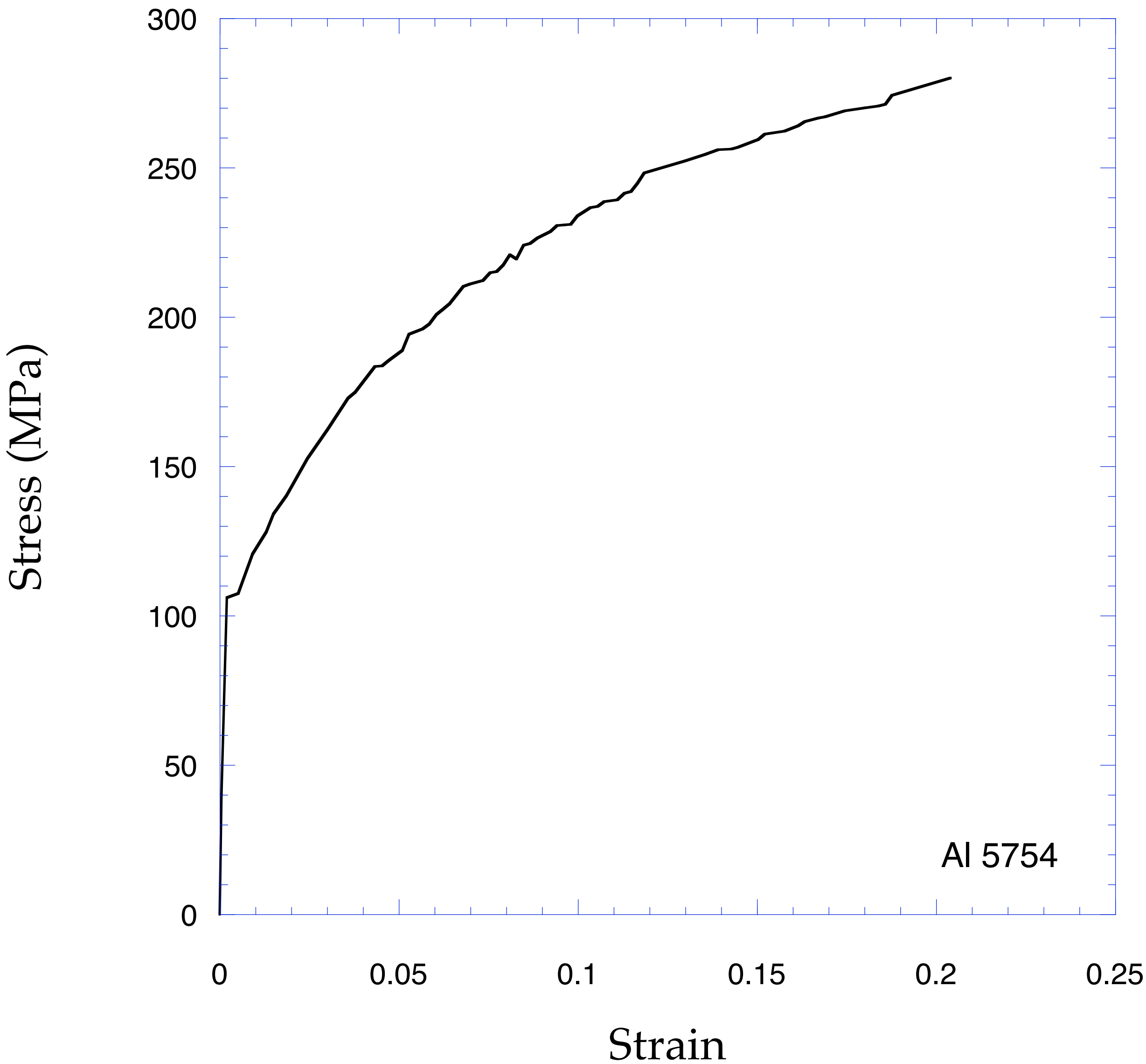
300
250
200
150
100
50
0
Stress (MPa)
0
0.05
0.1
0.15
0.2
0.25
Strain
Al 5754

Figure 2b

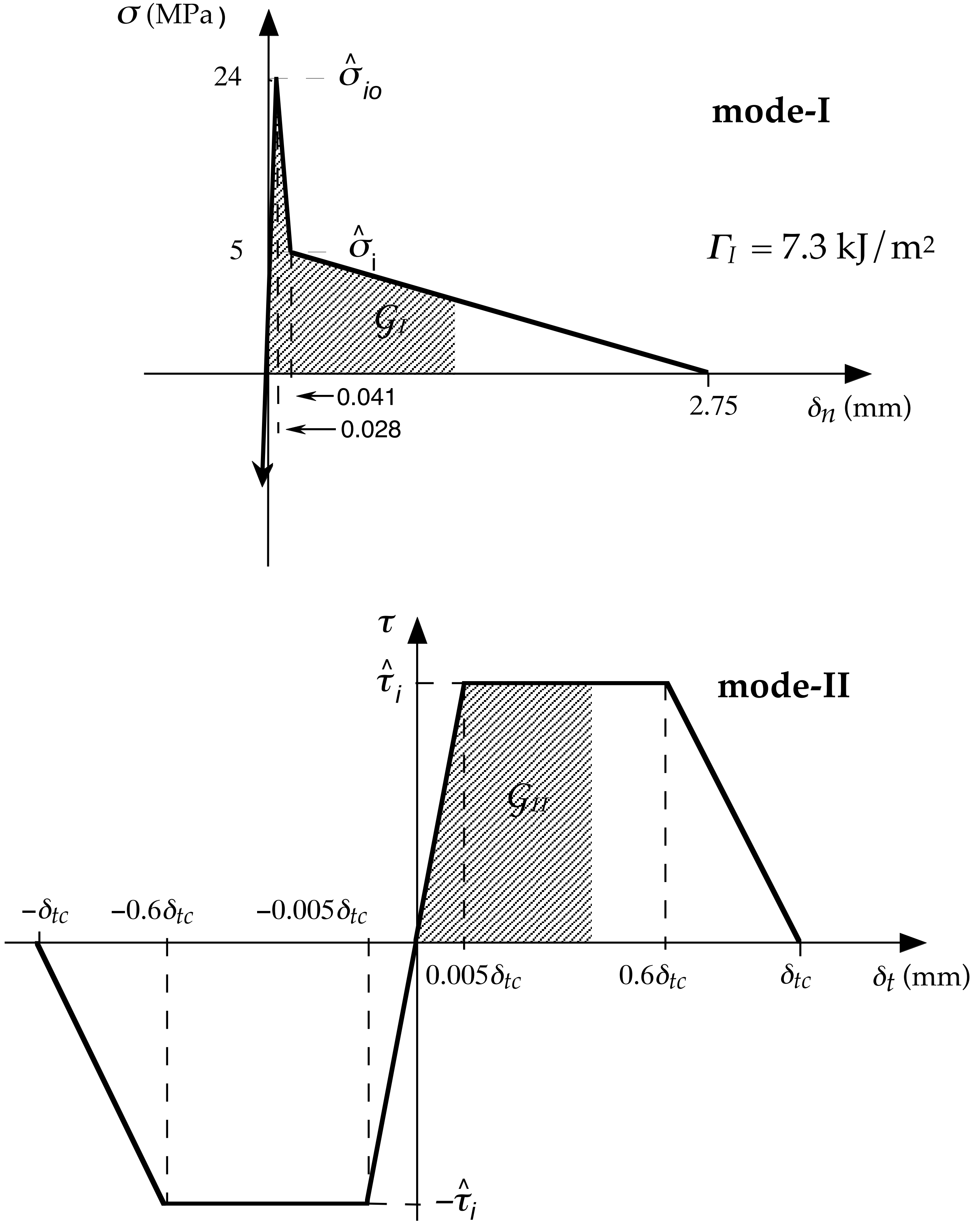

σ (MPa)
24
$\hat{\sigma}_{io}$
mode-I
5
$\hat{\sigma}_i$
$\Gamma_I = 7.3$ kJ/m2
$\mathcal{G}_I$
0.041
0.028
2.75
δ_n (mm)
τ
$\hat{\tau}_i$
mode-II
$\mathcal{G}_{II}$
$-\delta_{tc}$
$-0.6\delta_{tc}$
$-0.005\delta_{tc}$
$0.005\delta_{tc}$
$0.6\delta_{tc}$
δ_{tc}
δ_t (mm)
$-\hat{\tau}_i$

Figure 3

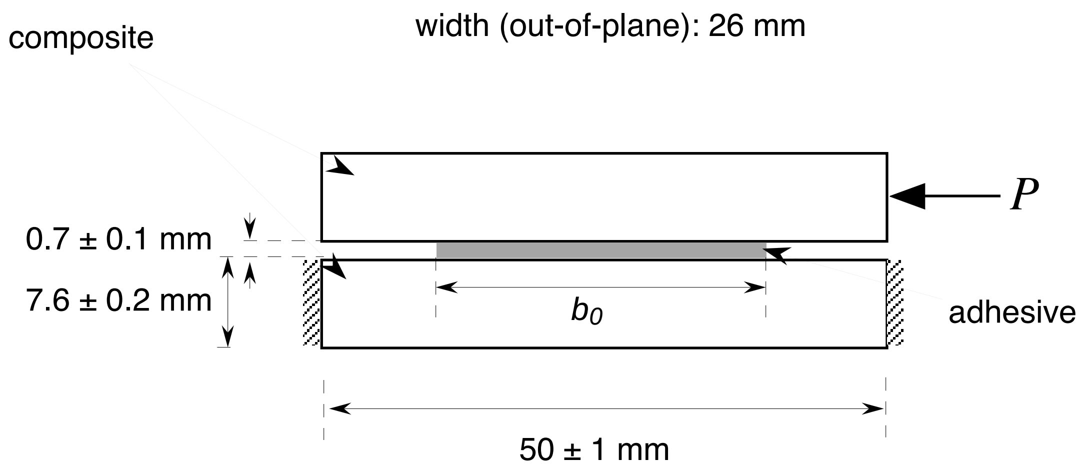
composite
width (out-of-plane): 26 mm
P
0.7 ± 0.1 mm
7.6 ± 0.2 mm
b_0
adhesive
50 ± 1 mm

Figure 4

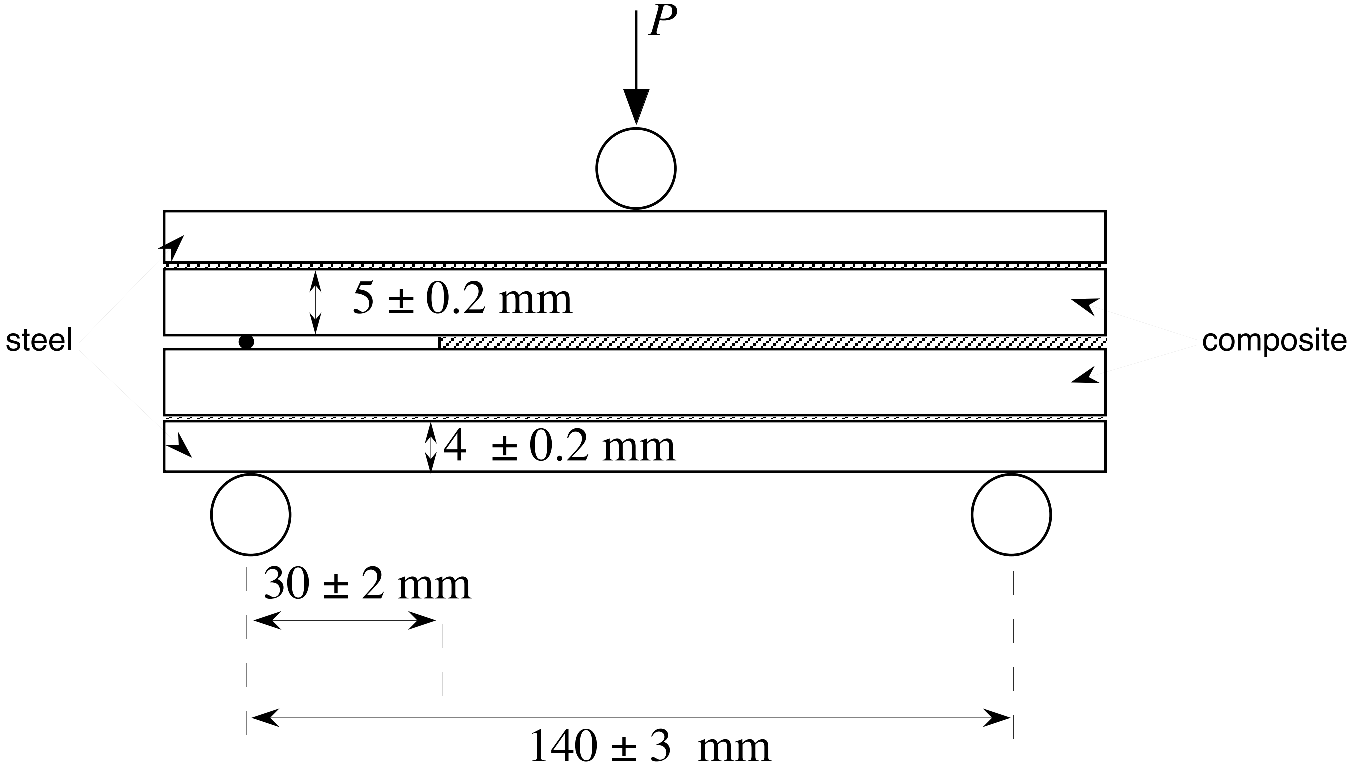

width (out of plane): 25 ± 0.5 mm

Figure 5

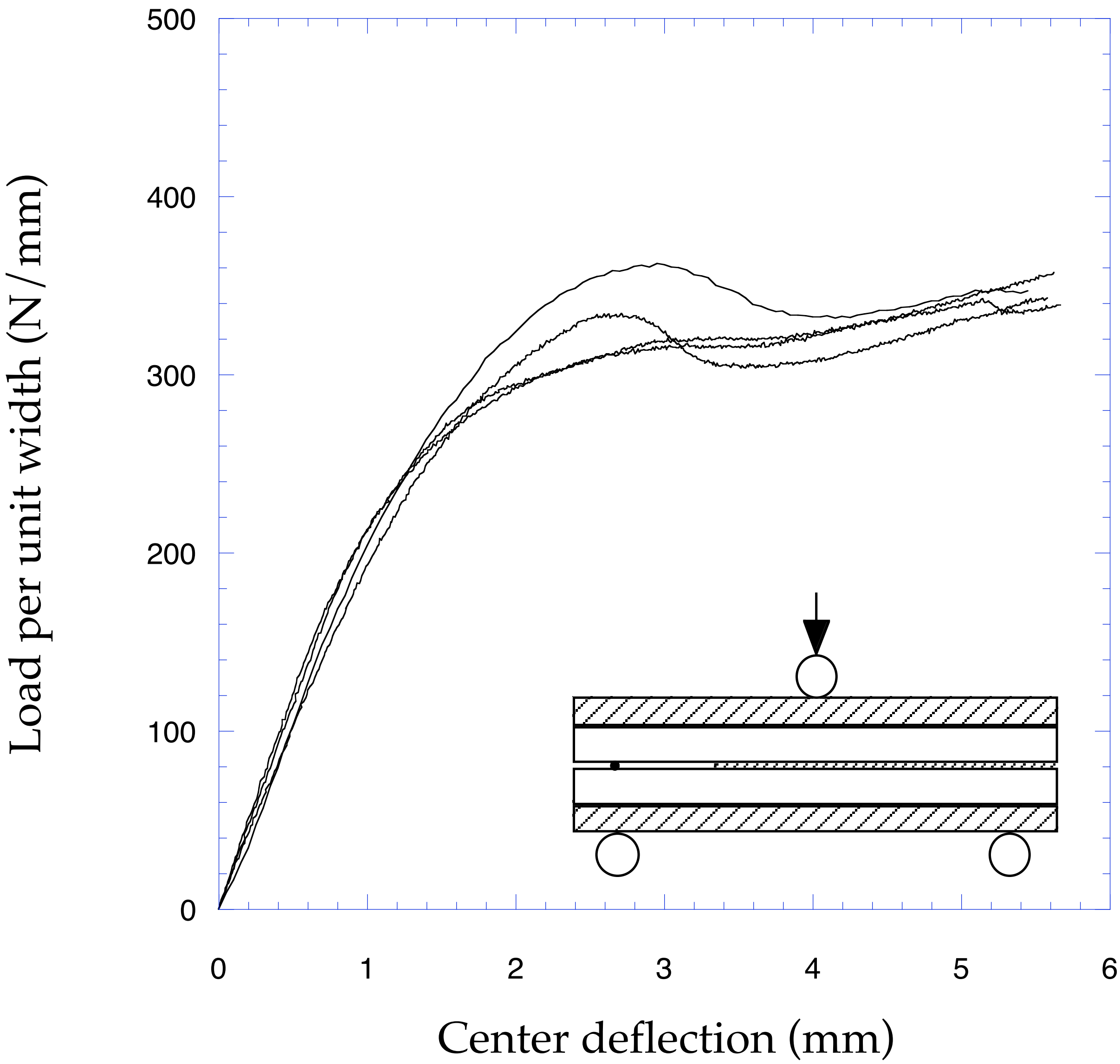

Load per unit width (N/mm)
500
400
300
200
100
0
0
1
2
3
4
5
6
Center deflection (mm)

Figure 6

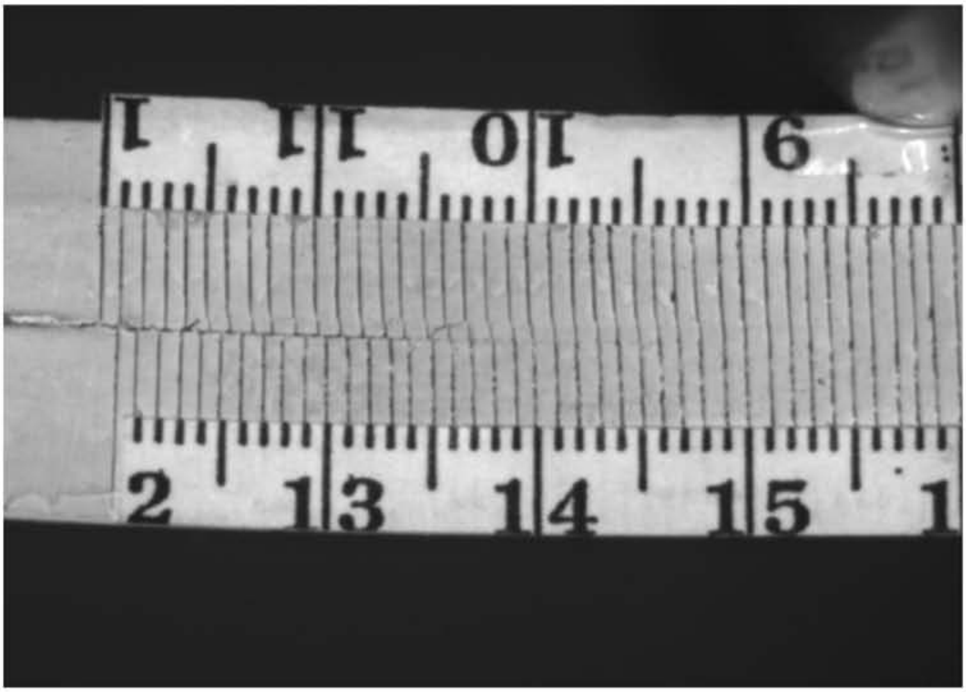

Figure 7a

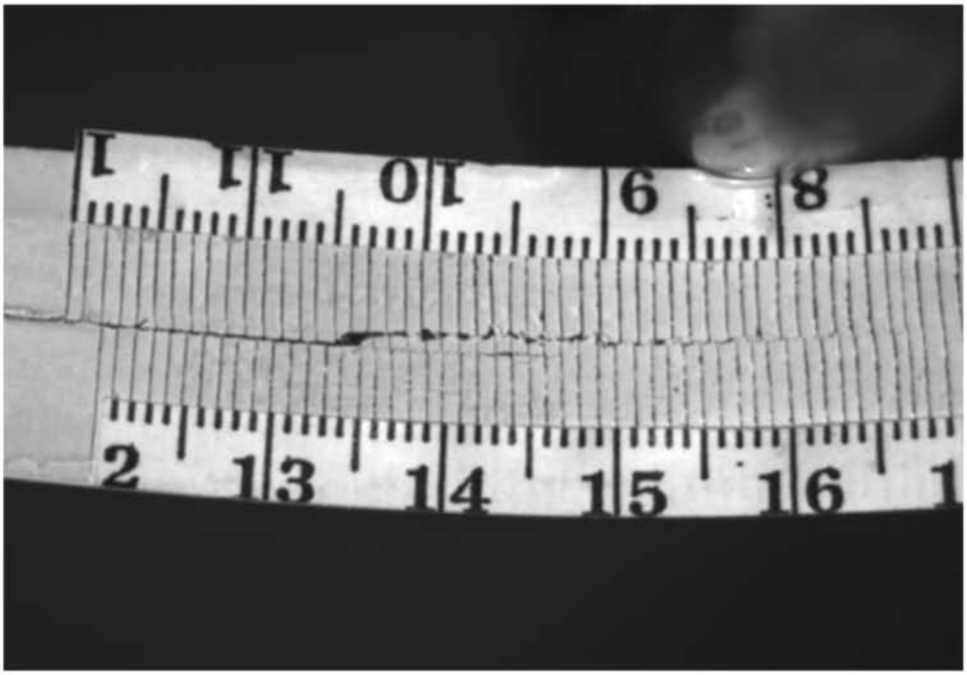

Figure 7b

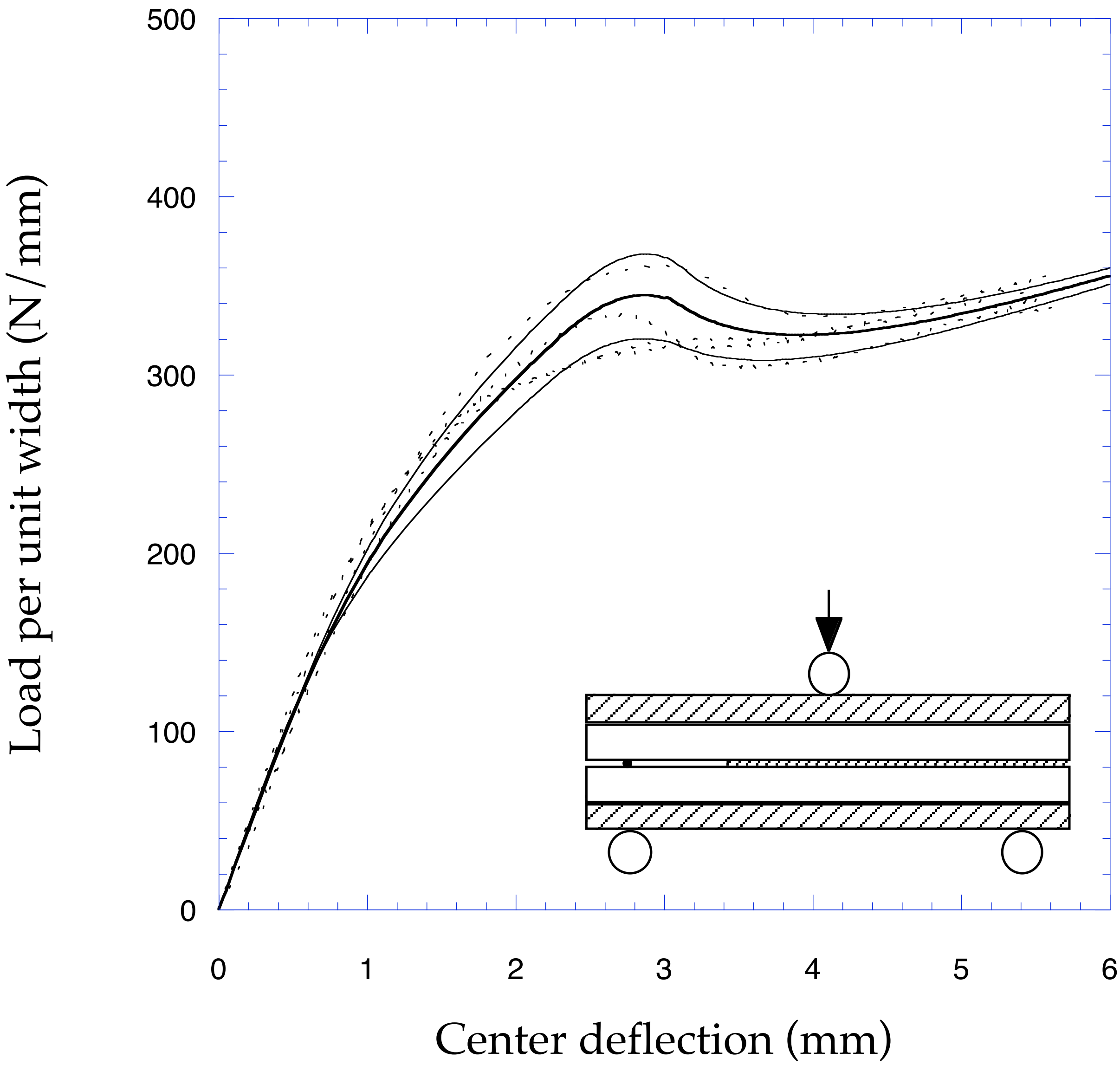

500
400
300
200
100
0
0
1
2
3
4
5
6
Load per unit width (N/mm)
Center deflection (mm)

Figure 8

width (out of plane): 20 mm

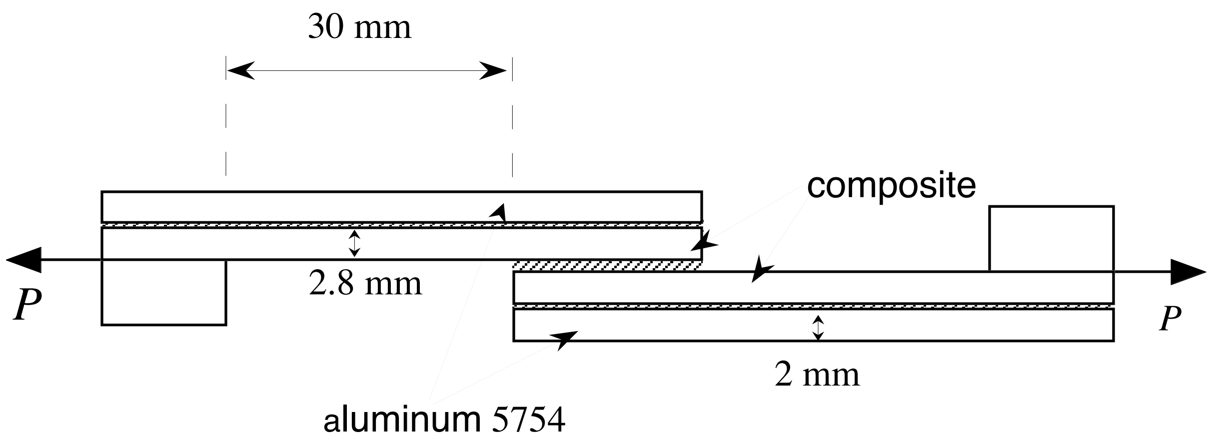

Figure 9

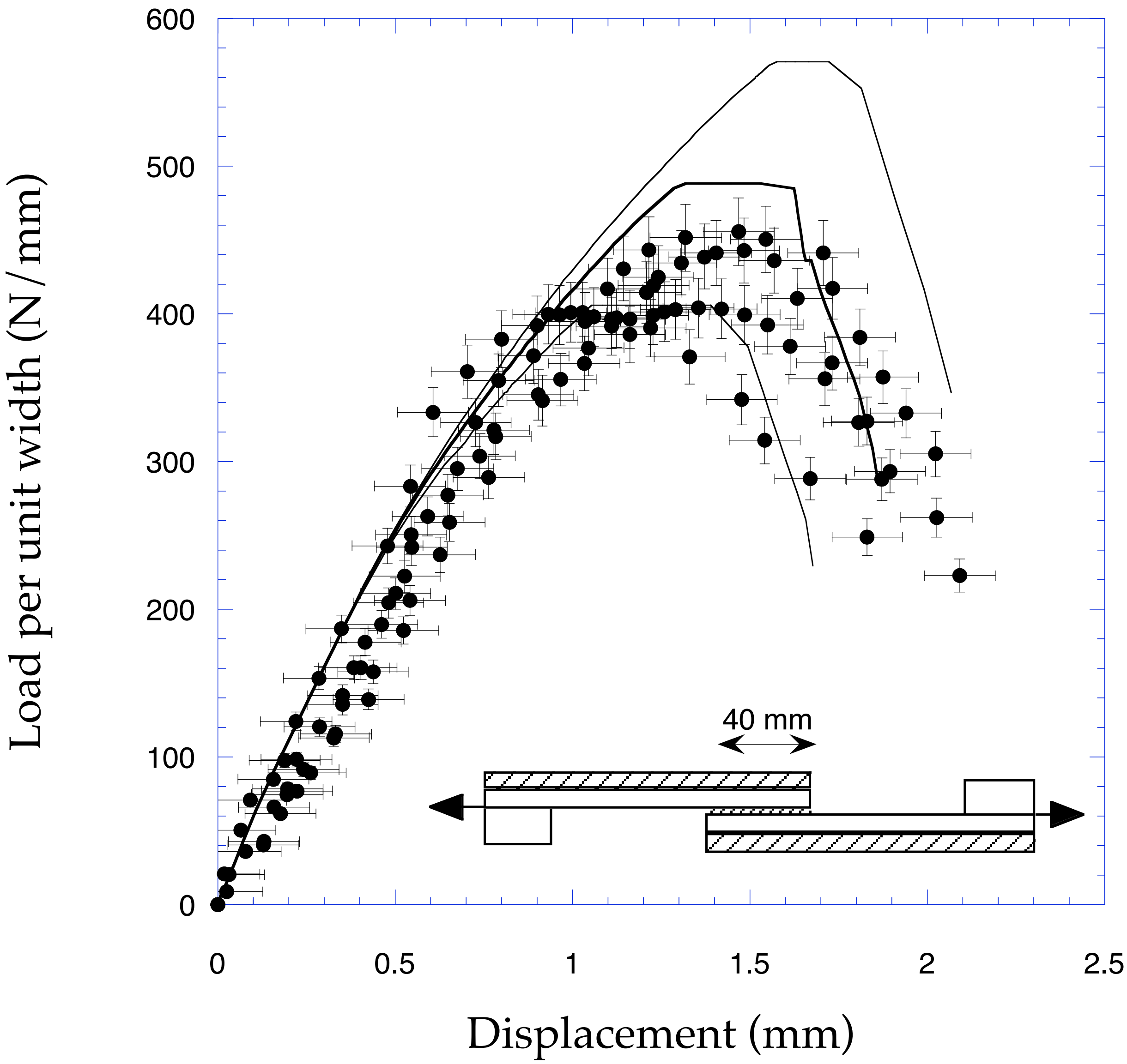
600
500
400
300
200
100
0
0
0.5
1
1.5
2
2.5
Load per unit width (N/mm)
Displacement (mm)
40 mm

Figure 10a

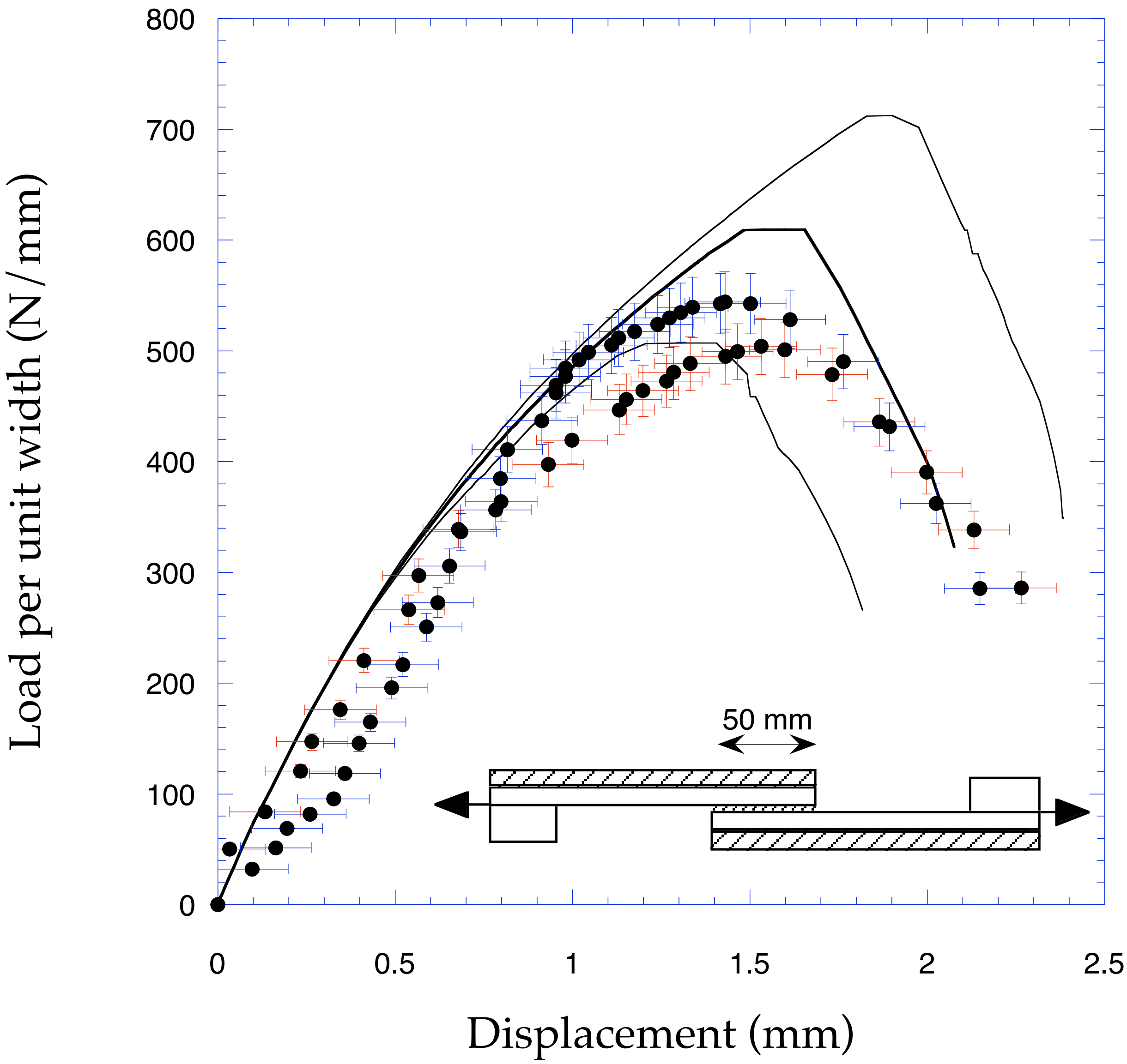
800
700
600
500
400
300
200
100
0
0
0.5
1
1.5
2
2.5
50 mm
Load per unit width (N/mm)
Displacement (mm)

Figure 10b

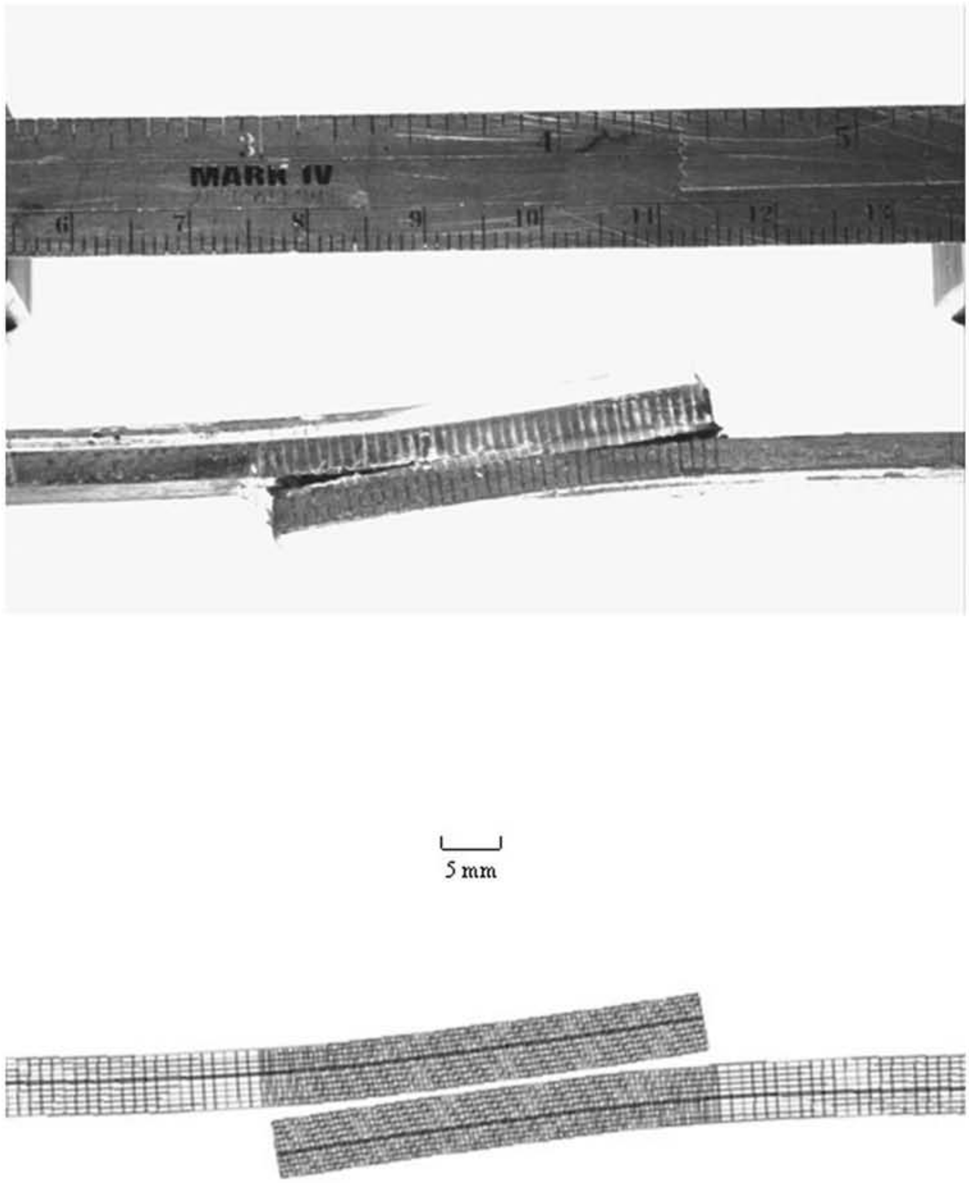

Figure 11

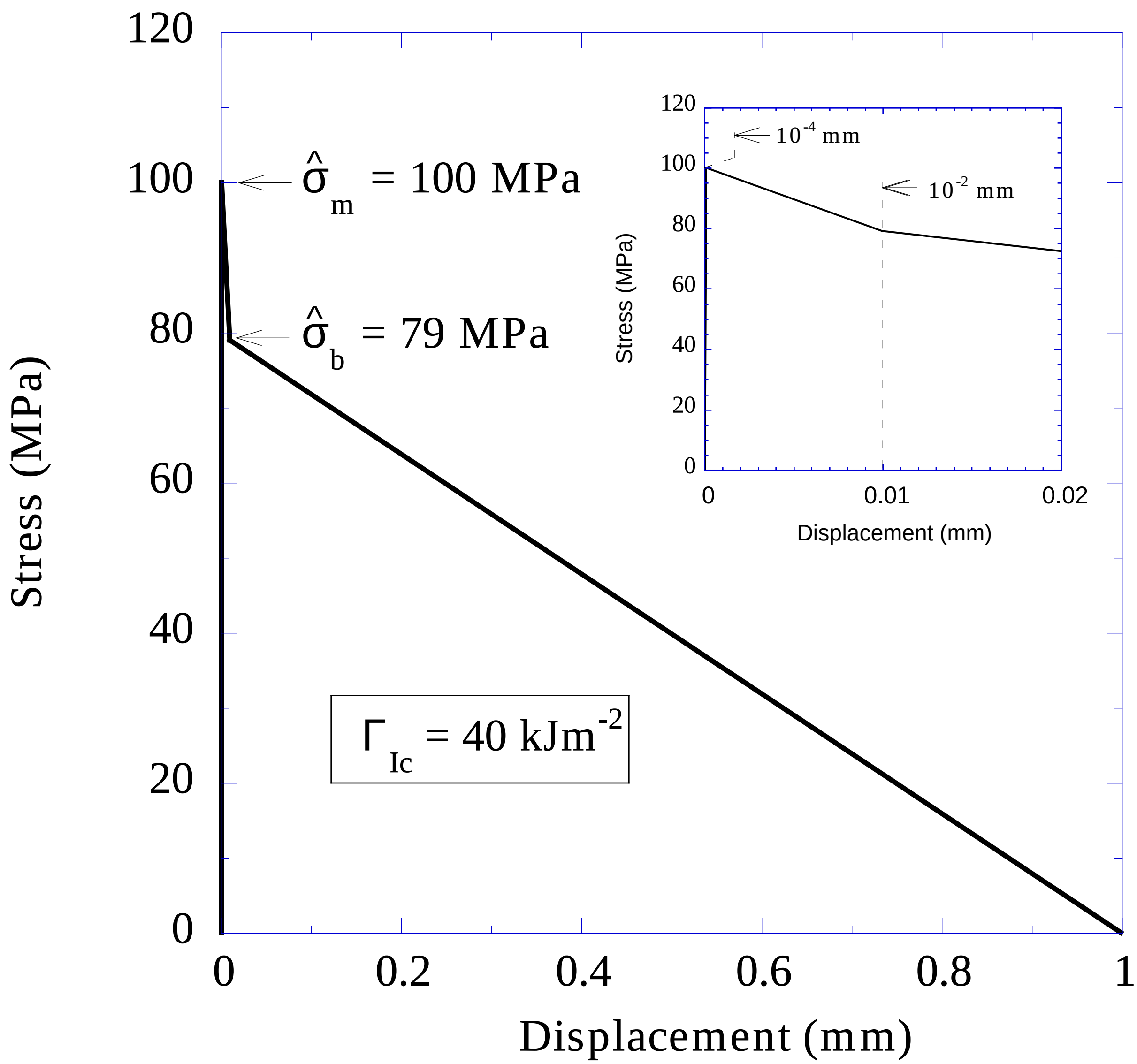

120
100
80
60
40
20
0
Stress (MPa)
0
0.2
0.4
0.6
0.8
1
Displacement (mm)
$\hat{\sigma}_m$ = 100 MPa
$\hat{\sigma}_b$ = 79 MPa
Γ_{Ic} = 40 kJm^{-2}
10^{-4} mm
10^{-2} mm
0.01
0.02

Figure 12

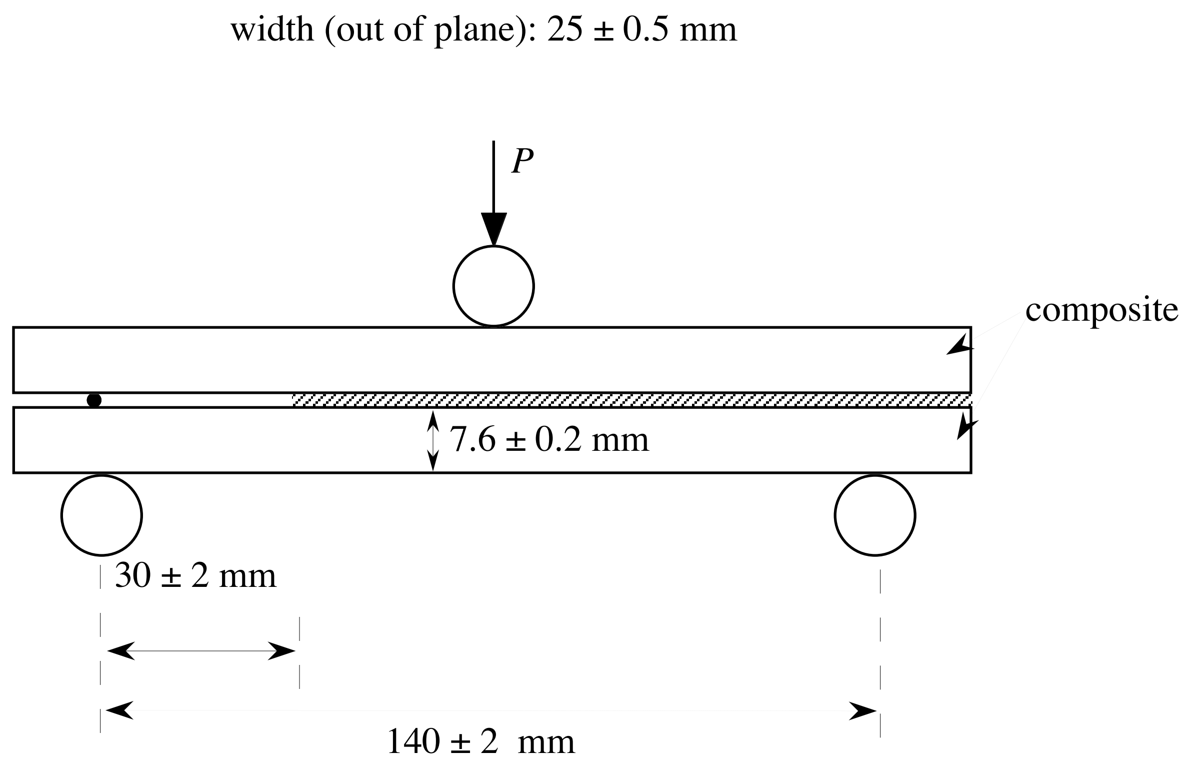

Figure 13

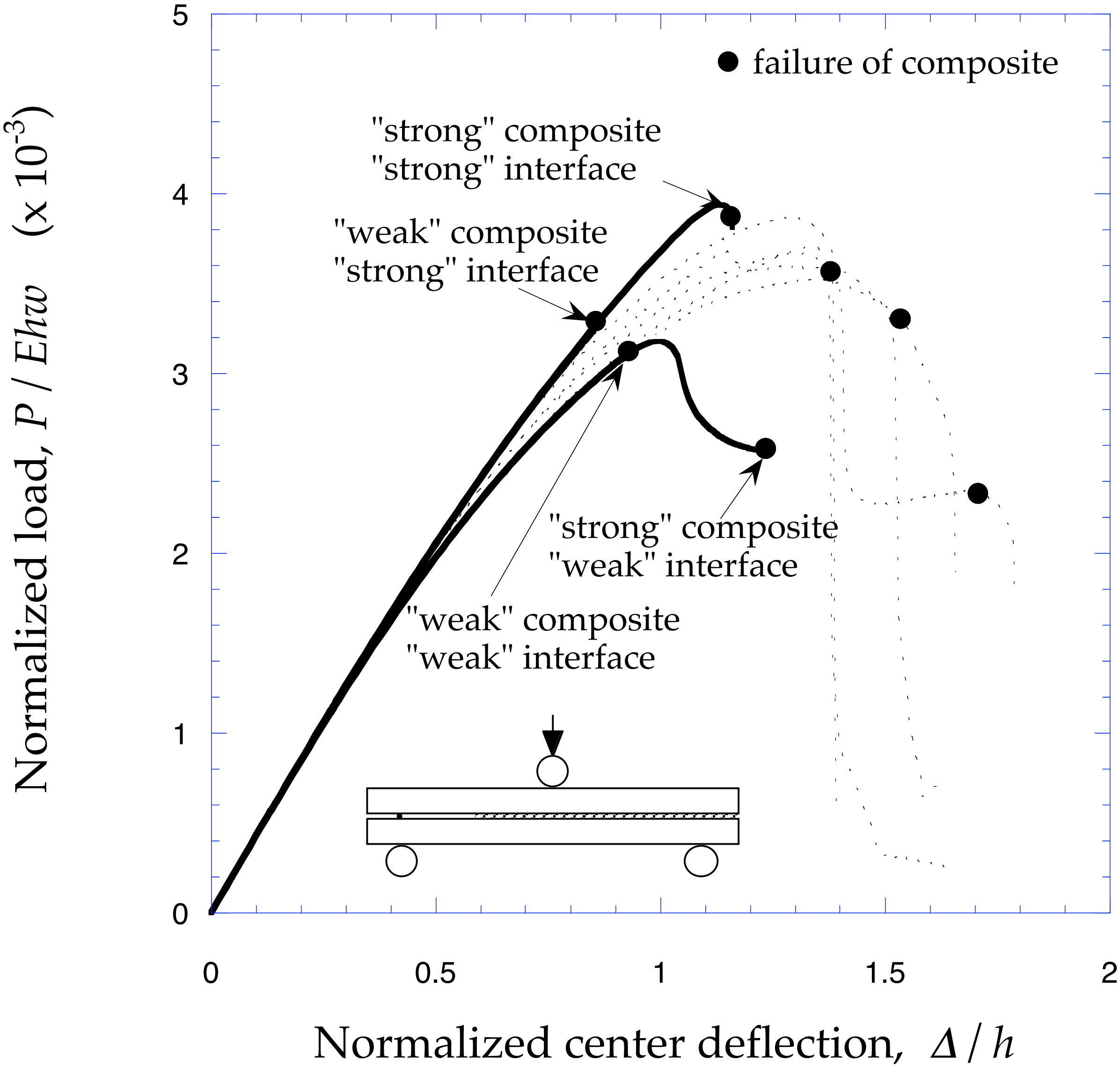

failure of composite
"strong" composite
"strong" interface
"weak" composite
"strong" interface
"strong" composite
"weak" interface
"weak" composite
"weak" interface
Normalized load, P / Ehw (x 10-3)
Normalized center deflection, Δ / h
0
1
2
3
4
5
0
0.5
1
1.5
2

Figure 14